Journal of Molecular Structure 1127 (2017) 99–113

Contents lists available at ScienceDirect

Journal of Molecular Structure

journal homepage: http://www.elsevier.com/locate/molstruc

Synthesis, stereochemistry determination, pharmacological studies and quantum chemical analyses of bisthiazolidinone derivative

Md. Mushtaque [a, *], Fernando Avecilla [b], Zubair Bin Hafeez [c, 1], Meriyam Jahan [a, 1], Md. Shahzad Khan [e, 1], M. Moshahid A. Rizvi [c, **], Mohd. Shahid Khan [d], Anurag Srivastava [e], Anwesha Mallik [f], Saurabh Verma [f]

[a] School of Physical and Molecular Sciences, Department of Chemistry, Al-Falah University, Dhauj, Faridabad, Haryana, 121004, India
[b] Departamento de Química Fundamental, Universidade da Coruña, Campus da Zapateira s/n, A Coruña, 15008, Spain
[c] Department of Biosciences, Jamia Millia Islamia, New Delhi, 110025, India
[d] Department of Physics, Jamia Millia Islamia, New Delhi, 110025, India
[e] Advanced Material Research Group, ABV-Indian Institute of Information Technology and Management, Gwalior, 474015, India
[f] National Institute of Pathology, Safdarjung Hospital Campus, New Delhi, 110029, India

ARTICLE INFO

Article history:
Received 17 June 2016
Received in revised form
17 July 2016
Accepted 20 July 2016
Available online 22 July 2016

Keywords:
Cytotoxicity
Cell cycle perturbation
DNA binding
Molecular docking and DFT studies

ABSTRACT

A new compound **(3)** bisthaizolidinone derivative was synthesized by Knoevenagel condensation reaction. The structure of synthesized compound was elucidated by different spectral techniques and X-ray diffraction studies. The stereochemistry of the compound **(3)** was determined by $^{1}H-^{1}H$ NOESY, $^{1}H-^{1}H$ NMR COSY and single crystal X-ray diffraction studies as *(Z, Z)*-configuration. The computational quantum chemical studies of compound(3) like, IR, UV, NBO analysis were performed by DFT with Becke-3-Lee-Yang-Parr (B3LYP) exchange-correlation functional in combination with 6−311++G(d,p) basis sets. The DNA-binding of compound **(3)** exhibited a moderate binding constant ($\mathbf{K_b = 1 \times 10^5\ Lmol^{-1}}$) with hypochromic shift. The molecular docking displayed good binding affinity **−7.18 kcal/mol**. The MTT assay of compound **(3)** was screened against different cancerous cell lines, HepG2, Siha, Hela and MCF-7. Studies against these cell lines depicted that the screened compound **(3)** showed potent inhibitory activity against HepG2 cell ($\mathbf{IC_{50} = 7.5\ \mu M}$) followed by MCF-7 ($\mathbf{IC_{50} = 52.0\ \mu M}$), Siha ($\mathbf{IC_{50} = 66.98\ \mu M}$), Hela ($\mathbf{IC_{50} = 74.83\ \mu M}$) cell lines, and non-toxic effect against non-cancerous HEK-293 cells ($\mathbf{IC_{50} = 287.89\ \mu M}$) at the concentration range (**0**−**300**) μM. Furthermore, cell cycle perturbation was performed on HepG2 & Siha cell lines and observed that cells were arrested in G2/M in HepG2, and G0/G1 in Siha cell lines with respect to untreated control. Hence, compound **(3)** possesses potent anti-cancerous activity against HepG2 cell line.

© 2016 Elsevier B.V. All rights reserved.

1. Introduction

Cancer is one of the deadliest diseases in human race ever seen [1]. According to world health organization (WHO), it is second most lethal disease causing deaths both in developing and developed countries [2]. All the developed, developing and under developed countries have constantly been afraid of this disease because it devastates both manpower as well as economy; thus creating havoc [3] for example, Asian countries like China and India along with Russia contribute more than half of the total cancer cases [4]. The current data of India show that every year, around 0.7 million people are losing their lives with one million new diagnosed cancer patients, which are estimated to be roughly doubled by the year 2035 [4]. Similarly, it is predicted that by 2030, approximately 20 million new cancer cases will be diagnosed worldwide and about 13 million cancer patients will die from this disease [3,5]. Indeed, many treatment modalities and drugs are available in the market to curb this terrifying disease like bio-alkylating (chloramethine) [6], anti-metabolic agents (fluorouracil) [7], anti-cancer antibiotics (doxorubicin) [8].

The anti-cancer drug development with less or no side effect is very important for chemotherapy of cancer. The necessity of such

** Corresponding author.
* Corresponding author.
E-mail addresses: mush.chem@gmail.com (Md. Mushtaque), rizvi_ma@yahoo.com (M.M.A. Rizvi).
[1] These authors contributed equally.

http://dx.doi.org/10.1016/j.molstruc.2016.07.089
0022-2860/© 2016 Elsevier B.V. All rights reserved.

potent anti-cancer therapeutic agents has led to discovery of small synthetic molecules which have anti-cancer activity with lesser side effects. Thiazolidone molecular scaffold is of great importance in modern medicinal chemistry, and is known to exhibit a diverse range of pharmacological activities like anti-cancer [9–12], anti-bacterial [13–15] Fig. 1(a&b), anti-fungal [16–18], anti-viral [19–22], and anti-HIV [23,24].

Previous studies on this class of molecule report excellent anti-amoebic activity with a high cytotoxicity [25]. In the view of versatile pharmacological importance, we herein, report the synthesis, characterization, DNA binding, molecular docking and DNA, cell cycle perturbation, and cytotoxicity. Also, a DFT study was carried out for evaluation of its biological potency of compound **(3).**

2. Results and discussion

2.1. Chemistry

The presented compound **(3)** (2Z, 2′Z, 5Z, 5′Z)-5,5′-(1,4-phenylenebis (methanylylidene)) bis(3-isopropyl-2-(phenylimino) thiazolidin-4-one), was synthesized by reported method [26]. The compound **(3)** was prepared in absolute ethanol using terephthaladehyde and thiazolidinone by Knoevenagel condensation reaction as shown in Scheme 1. The compound **(3)** is stable at room temperature and well characterized by different spectroscopic techniques; CHNS analysis, FT-IR, ^{1}H NMR, ^{13}C NMR and mass spectroscopy. The stereochemistry of compound **(3)** was determined by ^{1}H–^{1}H COSY-NMR and ^{1}H–^{1}H NOESY-NMR. Furthermore, stereochemistry was confirmed by X-ray single crystal structure.

The appearance and disappearance of the characteristic bands confirmed the formation of the compounds. In FT-IR, the appearance of the significant bands at 3265.14 cm^{-1} and 1240.83 cm^{-1} due to –NH and C═S confirmed the formation of compound (**1**). In ^{1}H NMR, the chemical shifts appeared at 8.267 ppm and 5.783 ppm due to presence of –NH protons, confirmed the formation of compound **(1).** Additionally, the compound **(1)** was confirmed by ^{13}C NMR. The presence of significant peak at 178.94 ppm was assigned to C═S, indicated the formation of compound **(1).** In case of intermediate compound **(2),** in IR, the appearance of characteristic bands at 1715.24 cm^{-1} and 1627.65 cm^{-1} due to –C═O and –C═N confirmed the formation of compound **(2).** In ^{1}H NMR, the presence of singlet at chemical shift 3.701 ppm due to the presence of-S–CH_2–C═O proton showed the formation of compound **(2).** The lead compound **(3)** was also confirmed by same spectroscopic techniques along with mass spectrometry and X-ray single crystal structure. In FT-IR, the presence of characteristic bands at 1704 cm^{-1} and 1629 cm^{-1} due to C═O and C═C confirmed the formation of compound**(3).** In ^{1}H NMR, the presence of characteristic peak resonated at high chemical shift at 7.631 ppm due to methylene (H–C═C-) proton confirmed the formation of compound **(3).** In ^{13}C NMR, the appearance of significant peaks due to C═O and C═C at 166.56 ppm and 148 ppm chemical shifts confirmed the formation of compound **(3)**. In mass spectrometry, the presence of $[M+H]^+$, $[M+2H]^+$ and $[M+3H]^+$ peaks at 567.18, 568.19 and 569.18 showed the formation of compound **(3).** Additionally, the structure of the compound **(3)** was confirmed by X-ray single crystal structure.

2.2. Stereochemistry and conformational properties

The determination of *E* or *Z*-configuration is important for compound **(3)** due to the presence of exocyclic C═N and C═C bonds. The configuration of compound **(3)** was determined by 2D-^{1}H–^{1}H COSY-NMR and ^{1}H–^{1}H NOESY-NMR. In ^{1}H–^{1}H COSY-NMR, the strong interactions were observed along off-diagonal peaks. The doublet due to methyl group at the range of 1.623–1.051 (ppm) chemical shift interacted with multiplet of CH at the range of 5.051–4.982 (ppm) chemical shift. But no off-diagonal peaks are present in the region of the aliphatic protons attached to the nitrogen of thiazolidinone ring and aromatic protons substituted at exocyclic nitrogen which could show correlation among them, indicating that the position of aromatic moiety adopted *Z*-configuration. Furthermore, there are strong interactions among the protons of exocyclic nitrogen substituted aromatic ring at chemical shifts range 7.432–7.349 ppm and 5-arylidene aromatic protons at chemical shift 6.990 ppm which confirms *Z*-configuration of exocyclic 5-arylidene. A *Z*-configuration of aromatic ring attached to exocyclic C═C bond of thiazolidinone derivative was further confirmed by a methine proton signal which resonated at a higher chemical shift 7.632 ppm as a singlet in ^{1}H NMR spectrum. The downfield chemical shift of the methine proton was due to deshielding effect of carbonyl group. Studies on *E*-configuration suggest the upfield resonance at chemical shift 6.6 ppm or less than δ 6.6 (ppm) [25–28]. In 2D NOESY ^{1}H NMR, the C═N imino and the C═C exocyclic double bond exhibited strong NOE signals at chemical shifts 7.432–7.349 ppm and 6.990 ppm due to the interaction of protons of two aromatic rings attached to imine (C═N) and 5-arylidene, indicating *Z*-configuration. No NOE signals were observed for exocyclic *N*-substituted aromatic protons and aliphatic (chain attached to the *N*-of thiazolidinone) protons which suggest that the molecule adopted Z-configuration. Additionally, a study of X-ray single crystal structure confirmed (*Z, Z*)-configuration Fig. 2.

2.2.1. Discussion of crystal structure

ORTEP diagram for the compound **(3)** (2Z,2′Z,5Z,5′Z)-5,5′-(1,4-Phenylene bis(methanylylidene))bis(3-isopropyl-2-(phenylimino) thiazolidin-4-one), was shown in Fig. 3. The asymmetric unit of **1**

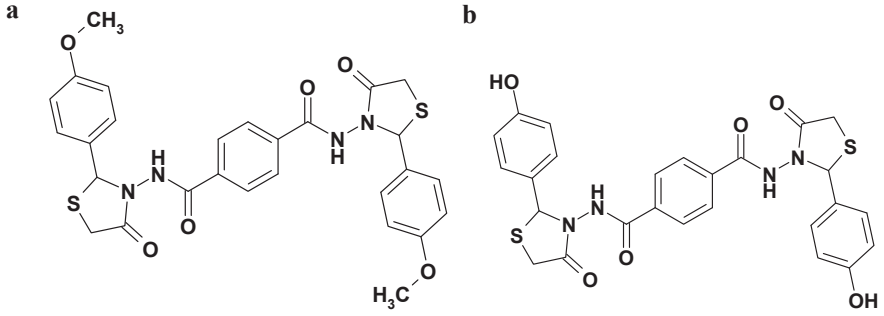

Fig. 1. (a–b): 4-Thaizolidinone derivatives (1 a & b) showing anti-bacterial.

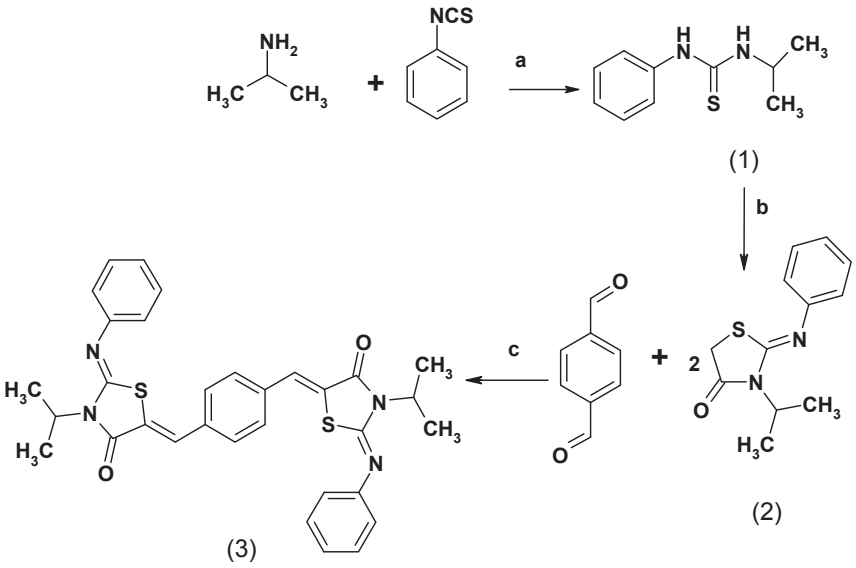

Scheme 1. (a) Toluene, Room temperature (b) Chloroacetic acid, Anhydrous sodium acetate, EtOH, reflux (c) Piperidine, EtOH Reflux.

contains only one molecule of compound **(3).** A Z-configuration of the exocyclic C═C and C═N bonds is observed in the structure. The phenyl ring [C15–C16–C17–C18–C19–C20] is not entirely flat with respect to the thiazolidinone rings[S1–C11–C12–C13–N2, torsion angle, 15.95(7)° and for S2–C22–C23–C24–N4, torsion angle, 18.55(7)°] and bonded to imine groups which are rotated with respect to the thiazolidinone rings[S1–C11–C12–C13–N2, torsion angle respect to C1–C2–C3–C4–C5–C6,68.15(3)° and S2–C22–C23–N3, torsion angle respect to C28–C29–C30–⊖ C31–C32–C33, 60.34(4)°]. The values of the bond lengths and angles are in agreement with those found in the similar derivatives [29]. Bond lengths and angles are summarized in Table (S1) (supplementary data). The crystal structure packing is mainly due to van der waals forces. Weak intermolecular hydrogen bonds between CH bonds of the phenyl rings and the methylidene groups with O atoms of thiazolidin-4-one groups are observed in the crystal packing (Fig. 3) [30]. Weak intramolecular and intermolecular hydrogen bonds between the methyls of the propyl groups, O atoms of thiazolidin-4-one groups and N atoms of the imine groups determine the configuration of the structure around C═C and C═N bonds Table 1. Also, weak hydrogen bonds between CH groups and π clouds of the terminal phenyl rings appear in the crystal packing (see Fig. 3) [31].

2.3. Computational details

The ground state optimization of compound **(3)** has been carried out using DFT with Becke-3-Lee-Yang-Parr (B3LYP) exchange-correlation function [32,33] in combination with 6–31++G(d,p) basis sets using Gaussian03 package [34] without any symmetry constraint. The NBO and Mulliken population analysis are also reported for the local minima of a molecule. For electronic excited state calculations, TD-DFT/B3LYP method has been employed with the same basis set considered for ground state optimizations. The simulated IR spectrum was analyzed by GAUSSVIEW and VEDA 4 program to assign vibrational frequencies with high degree of accuracy. Molecular electrostatic potential of the molecules have also been presented to view electrophilic and nucleophilic reactive sites.

2.3.1. NBO analysis

The NBO analysis was carried out by 6–311++G(d,p) basic set

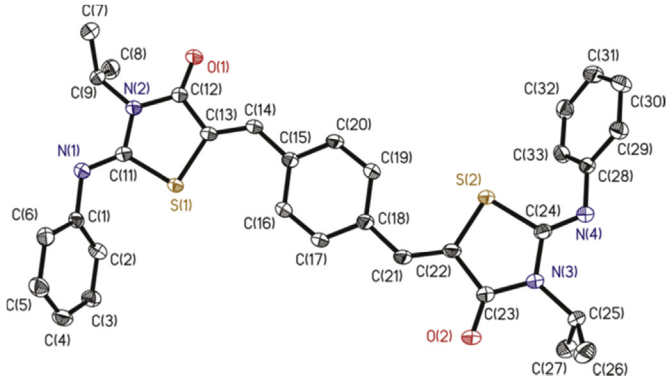

Fig. 2. X-ray single crystal structure of compound **(3)**.

with help of optimized geometry and is represented in Fig. 4. NBO analysis illustrates role of intra and intermolecular bonding interactions. It also provides suitable base for investigation of charge transfer or hyper conjugative interactions in molecular system. The energy difference between interacting orbitals is proportional to stabilization of orbital interaction. Hence, the strongest interaction of stabilization occur between dominant donor (i) and acceptor (j). Quantitatively, interaction between bonding and anti-bonding orbitals is described in terms of NBO basis, and is expressed by means of second order perturbation interaction energy, E(2) [35]. This energy depicts an estimate of the off diagonal NBO Fock matrix element. The stabilization energy is calculated by following mathematical expression:

$$E^2 = \Delta Ei,j = qi\frac{F(i,j)2}{\varepsilon i - \varepsilon j} \quad (1)$$

where qi is donor orbital occupancy, εi and εj are diagonal elements (orbital energy) and F(i, j) is off diagonal Fock matrix. The NBO analysis has been carried out on entitled compound **(3)** using Gaussian 03 package at the B3LYP/6-311G(d,p) level for illustrating intramolecular charge transfer and delocalization of electron density within molecule. The significant interactions between donor NBO orbitals and acceptor orbitals of compound **(3)** are given in

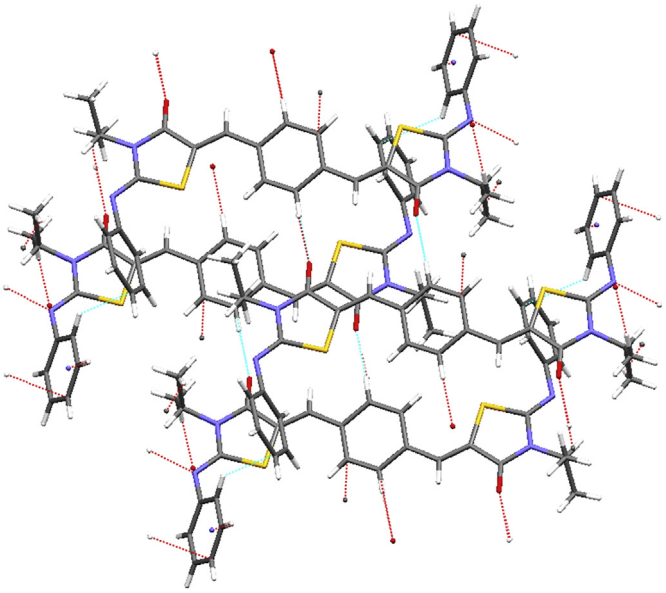

Fig. 3. Crystal packing in the compound **(3)**. Blue dashes lines show some C–H···O and C–H···π hydrogen bonds. (For interpretation of the references to color in this figure legend, the reader is referred to the web version of this article.)

Table 2. It was found that lone pair of electron present on sulphur atom delocalized into anti-bonding molecular orbitals of π*(N3–C30) and π*(C32 – C33) through hyper conjugation and gives stabilization energy of **23** kcal/mol and **21** kcal/mol. However, lone pair of electrons present on N3, N7 and N10 interacts with anti-bonding orbital of σ*(S1–C30), π*(O2–C31) and π*(N13–C49) through hyper conjugation, causing stabilization energy 25 kcal/mol, 58 kcal/mol and **47** kcal/mol respectively. The lone pair of electron present on O2 interacts with anti-bonding orbital σ*(N7–C31) through resonance and gives stablization energy **27** kcal/mol. The π-bonding electron of π(C32–C33) interacted with the anti-bonding orbital of π*(O2–C31) through hyper-conjugation, causing stablization energy **20** kcal/mol, and π-bonding orbital of π(C16–C18) interacted with the anti-bonding orbital of π*(C4–C8) through resonance and caused stabilization energy **21** kcal/mol. Thus, whole molecule is stabilized by hyper-conjugation and resonance.

2.3.2. Frontier molecular orbitals

The biological potency of a molecule can be described in terms of the highest occupied molecular orbital (HOMO) and the lowest unoccupied molecular orbital (LUMO). The small interfrontier orbital of a molecule is chemically more active and has low kinetic stability [36–39]. The highest occupied molecular orbital (HOMO) directly corresponds to ionization potential. However, the lowest unoccupied molecular orbital corresponds to electron affinity (electron gain enthalpy) of a molecule [41]. The HOMO and LUMO orbitals have been shown in Fig. 5(a). These two orbitals are very significant to understand the potency of a molecule by calculating chemical potential, global hardness and electronegativity. The ionization energy and electron affinity are expressed as $I = -E_{HOMO}$ and $A = -E_{LUMO}$, respectively. The chemical potential and hardness are derived by mathematical expression; $\mu = -(I + A)/2$ and $\eta = (I-A)/2$. The compound **(3)** has $E_{HOMO} = -$**5.7eV** and $E_{LUMO} = -$**2.58eV**. Subsequently the associated μ and η are **−4.15ev** and **−1.6eV**, respectively. The stability is presented by negative chemical potential. The hardness of the title molecule is **1.6eV** and believed to be soft or chemically active. The energy gap between HUMO and LUMO of molecule is **3.142** eV as shown in Fig. 5(b).

Table 1
Weak intermolecular and intramolecular hydrogen bonds in the compound **(3)**.

D-H···A	d(D-H)	d(H···A)	d(D···A)	<(DHA)
C(7)-H(7C)···O(1)	0.98	2.52	3.0691(15)	115.1
C(8)-H(8A)···O(1)	0.98	2.56	3.1381(16)	117.6
C(8)-H(8C)···O(2)[a]	0.98	2.72	3.6578(17)	159.6
C(9)–H(9)···N(1)	0.965(14)	2.343(14)	2.8595(15)	112.8(10)
C(14)–H(14)···O(2)[b]	0.930(15)	2.953(15)	3.7467(14)	144.1(11)
C(21)–H(21)···O(1)[c]	0.940(14)	2.991(14)	3.7865(14)	143.3(11)
C(25)–H(25)···N(4)	0.955(16)	2.367(16)	2.8660(15)	112.1(11)
C(26)-H(26A)···O(1)[d]	0.98	2.53	3.5017(18)	172.7
C(26)-H(26C)···O(2)	0.98	2.48	3.0446(16)	116.5
C(27)-H(27A)···O(2)	0.98	2.58	3.1290(16)	115.8

Symmetry transformations used to generate equivalent atoms.
[a] −x+1,−y,−z+1.
[b] x,y+1,z.
[c] x,y−1,z.
[d] −x,−y,−z+1.

2.3.3. Relation between theoretical and experimental UV–visible

Due to high accuracy and low computational cost, TD-DFT is widely used of for electronic spectra transitions. The experimental and simulated UV–Visible absorption spectra of compound **(3)** have been shown in Fig. 6(a–b). The vertical excitation energies, oscillator strength (f) and transition wavelength along with assignments have been mentioned in Table 3. The experimental wavelength was observed at **400** nm having absorbance of 3.02. However, its theoretical counterpart was calculated at **449** nm associated with oscillator strength of 1.42. This electronic transition is majorly associated with HOMO to LUMO with 86.5% contribution. As it is clear from Fig. 7, HOMO electron density is delocalized over the whole molecule, which means HOMO→LUMO transition results in the electronic density to confine at the central benzene ring. Canonical molecular orbitals output from the G03 software package suggests that these frontier molecular orbitals (FMOs) mainly consist of p orbital, hence this transition is π→π* in nature (extended conjugation). Transition observed at **256** nm is qualitatively in good agreement to the calculated value of **256** nm which is both π→π* and n→σ* in nature. The contribution of electronic excitations from HOMO and HOMO-3 to LUMO+2, LUMO+5 and LUMO+1 contribute this transition. The other two important transitions which are calculated in between these two extremes are **381** nm and **293 n**m. The former result to the significant electronic charge shifting from thiazolidinones to the central benzene ring and is π→π* in nature, this transition involves electronic excitation from HOMO-2 to LUMO orbital having a contribution of 92%. However, later one has combinatorial nature of n→π* and π→π* transitions. The experimental electronic transitions at **370** nm and **280** nm correspond to these calculated transitions of **381** nm and **293** nm.

2.3.4. IR analysis

The compound **(3)** consists of 70 atoms which consequence to 204 normal modes of fundamental vibrations. This molecule belongs to C1 symmetry. Up to the best of our knowledge none have reported the quantum chemical study for molecular structures and IR-spectra of compound **(3).** The observed and calculated IR-spectra have been presented in Fig. 8 and comparison has been demonstrated in Table 4. The rigorous analyses for fundamental modes of vibrations with B3LYP have been shown in Table 4. In our study, we have scaled the B3LYP calculation with 0.98 to correct the theoretical error.

2.3.4.1. C–H vibrations. The C–H stretching vibration from

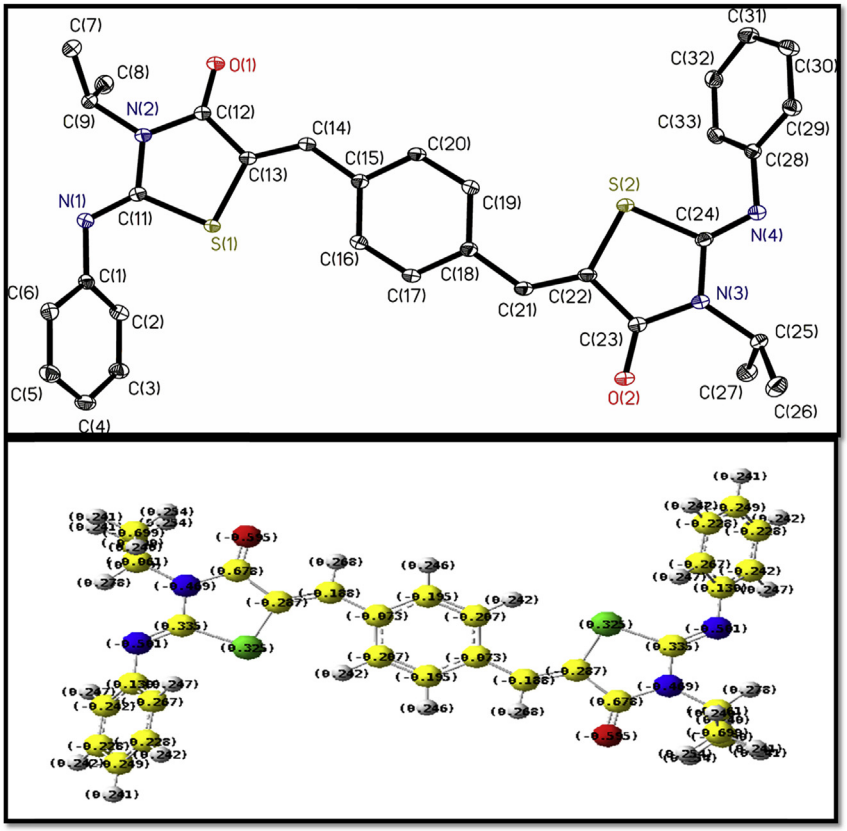

Fig. 4. XRD structure and optimized geometry of compound **(3)** Numbers display on atoms of optimized molecule is natural charges obtained by NBO calculation.

Table 2
Second order perturbation theory analysis of Fock matrix in NBO basis corresponding to some the intra-molecular bonds of compound**(3)**.

Donor(i)	Acceptor(J)	E^2(Kcal/mol)
LP(2)S1	π*(N3 − C30)	23
LP (2)S1	π*(C32–C33)	21
LP(1)N3	σ*(S1–C30)	25
LP(1)N7	π*(O2 − C31)	58
LP(1)N10	π*(N13 − C49)	47
LP(2)O2	σ*(N7–C31)	27
π(C32–C33)	π*(O2–C31)	20
π(C16–C18)	π*(C4–C8)	21

different location of compound (**3**) falls in the region of 3054–3201 cm^{-1}. The C–H vibration of terminal methyl group contributes to the peaks at 3055 cm^{-1}, 3123, 3126 cm^{-1} and 3160 cm^{-1}. The C–H stretching vibrations of benzene rings are dispersed on modes at 3223, 3212, 3207, 3201.20 and 3188 cm^{-1}. The C56–H57 and C52–H53 stretching vibration contribute at wavenumber 3160 cm^{-1} and 3126 cm^{-1} with 74% and 90% contributions. The C20–H21 stretching contributes at wavenumber 3055 cm^{-1} with 86% contribution. C52–H53, C52–H54, C56–H58 and C56–H59 stretching contribute wavenumber at 3126 cm^{-1} with 12% contribution. The C61–H62 stretching contributes at 3212 cm^{-1} with 72% contribution and rests have been given in Table 4. These vibrational modes in particularly assigned in our experimental observation collectively at 3089 cm^{-1}, 3034 cm^{-1}, 2977 cm^{-1}, 2936 cm^{-1} and 2880 cm^{-1}. The other mode of vibrations like bending, torsion and out of plane of bending modes has been summarized in Table 4.

2.3.4.2. C=O vibrations. Theoretically, the O–C stretching vibration of C=O of thiazolidinone ring is assigned at wavenumber 1783 cm^{-1}. However, its experimental counterpart was observed at

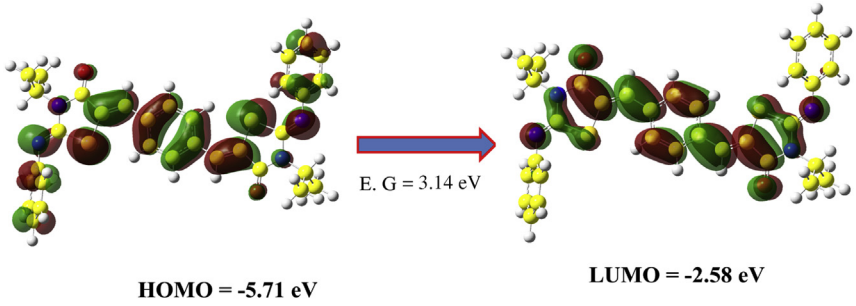

Fig. 5. Frontier molecular Orbitals of compound **(3)**.

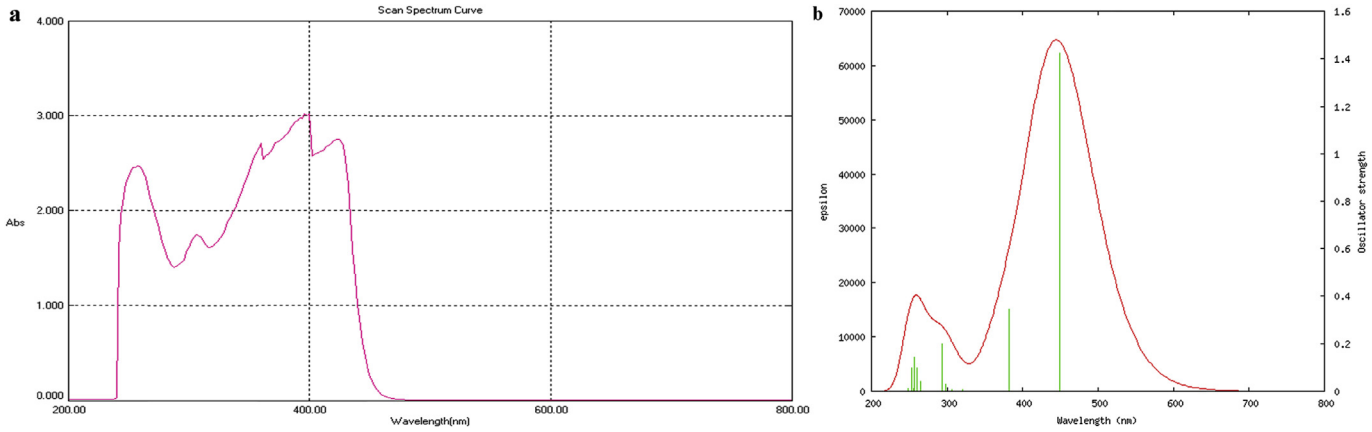

Fig. 6. (a&b): Experimental (a) and theoretical (TFDFT-B3LYP/6-31g(d,p)) UV–Vis spectra of compound(**3**).

Table 3
Comparative study between experimental and theoretical UV-Visible in chloroform background of compound(**3**).

Experimental			TD-B3LYP	
λ_{nm}	Abs	λ_{nm}	Oscillator Strength	Assignments
400	3.02	449	1.4	HOMO − LUMO(86.5%) $\pi \rightarrow \pi^*$
370	2.80	381	0.34	HOMO-2 − LUMO(92%) $n—\pi^*$
280	1.44	293	0.19	HOMO-6 − LUMO(54.2%) $n \rightarrow \pi^*$ HOMO-1− LUMO+1(31%) $\pi \rightarrow \pi^*$ HOMO-3− LUMO+1(21.4%) $\pi \rightarrow \pi^*$
256	2.04	256	0.14	HOMO − LUMO+2(22.2%) $\pi \rightarrow \pi^*$ HOMO − LUMO+5(19.6%) $n \rightarrow \sigma^*$

1704 cm^{-1}. The out of plane vibration of O2–C32–N7–C31, O2–C32–N7–C31, O6–C47–N10–C48, O2–C32–N7–C31 of thiazolidinone ring contribute wavenumber at 735 cm^{-1} and 725 cm^{-1} and 752 cm^{-1} respectively. The experimental results for these vibrations were observed at 735 cm^{-1} and 764 cm^{-1} respectively.

2.3.4.3. C=C vibrations. The theoretical stretching vibrations associated with alkenic carbon (C=C) was found at 1630 cm^{-1} with contribution of 50%. However, experimental vibration was observed at 1629 cm^{-1}.

2.3.4.4. C–N–C vibrations. The C–N–C bending vibration due to C4–N3–C30 and C28–N7–C31 contribute wave number at 905 cm^{-1}. The experimental result was found at 911 cm^{-1}.

2.3.4.5. C=N vibrations. The calculated C–N stretching vibrations are observed in combination with other vibration modes and are dispersed in the range of 1136–1377 cm^{-1}. The C–N stretching vibration due to N3–C30, N7–C30 and N7–C31 contribute at wave number 1315 cm^{-1}. The experimental wave number was observed at 1592 cm^{-1}. The other modes of vibrations have been depicted in Table 4.

2.3.5. Comparison between theoretical and experimental bond angles and bond length

The theoretical bond angles and the bond lengths obtained by DFT calculation have been compared with the experimental results. From Tables TS1 & TS2 (Supporting information), it was observed that the theoretical and experimental results are almost same. A few deviations from experiment results have also been observed. The experimental angle of C (11)-N (1)-C (1) was 117.70°. However, its theoretical bond angle was 123.123°. The bond angle of C (24)-N(4)-C (28) was observed at 118.31°. However, its theoretical bond angle was 123.123°. The bond angle of C (13)-C (14)-C (15) was 129.63° and its theoretical bond angle was 131.758°.

2.3.6. Molecular electrostatic potential (MEP)

Molecular electrostatic potential (MEP) is a useful descriptor to describe the chemistry of a designed molecule in quantum chemical simulation and is based on electron density (ED). It helps in finding the active electrophilic and nucleophilic sites along with hydrogen bonding [40]. The mapping of electrostatic potential to the total electron density in the framework of ab-initio calculation results the 3D image visualization in GaussView4 graphical interface. The electron rich (negative potential) region has been coded with red color and electron deficient (positive potential) region has been coded with blue color. The zero potential surfaces have been coded with Green color. Other colors have represented in between the limits of red and blue. The electrophilic potential increases in the order of red < orange < yellow < green < blue. It could be inferred from Fig. 9 that, dangling oxygen at 4-thiazolidinone-rings is an electron rich center and the terminal hydrogen at benzene ring has a positive electron cloud and could be consider as protonation of these hydrogen atoms. So these sites can serve as a good attractor for electrophilic and nucleophilic species and are comparatively more chemically active than other molecular regions.

3. Pharmacological activities

3.1. DNA binding

DNA is one of the most important targets for many pharmaceutically active agents including anticancer drugs. Many organometallic and organic moieties are well known which bind to DNA in different ways [41–43]. Hence, study of interaction of new compounds with DNA would be a promising step for the development of new drugs. For this purpose, UV–Visible spectroscopy is one of the most commonly employed techniques [43]. In UV–Visible spectrophotometric titration, hypochromic and hyperchromic shifts with change in wavelength, absence or presence of isosbestic points are the characteristic of interactions of compounds with

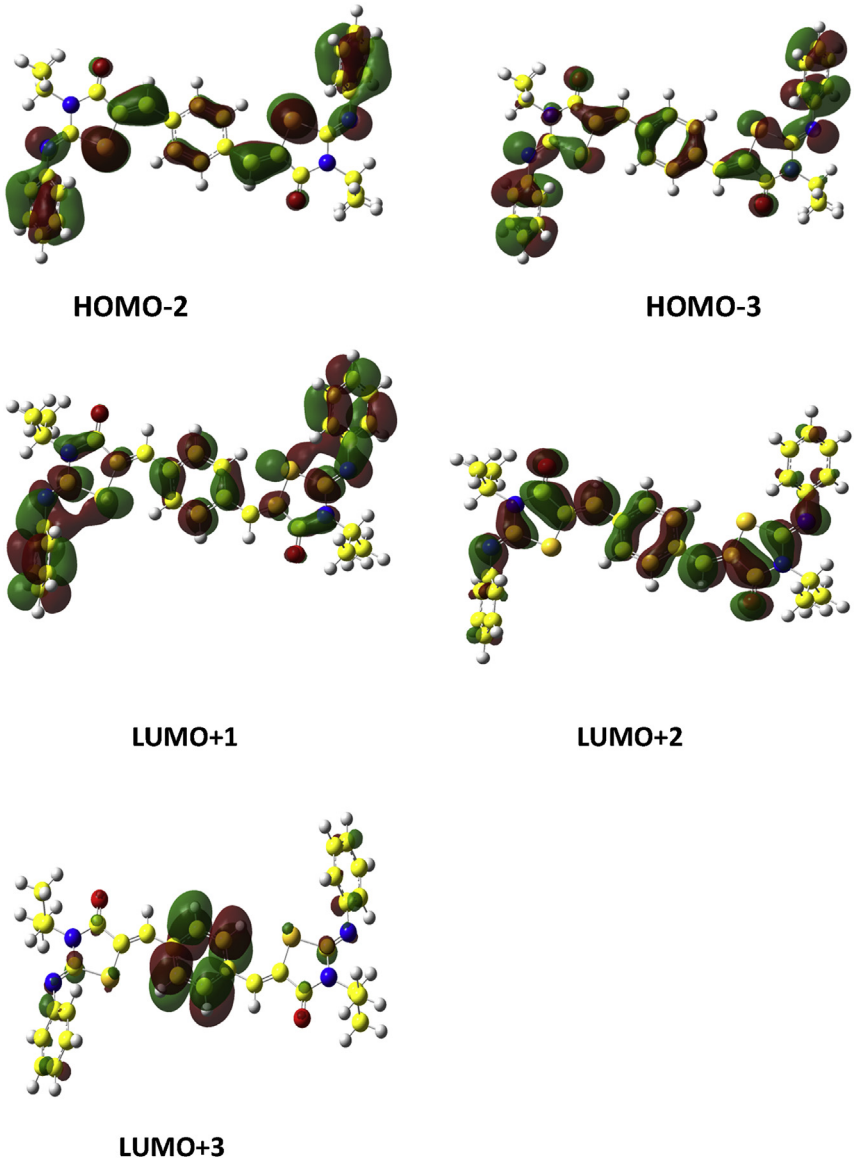

Fig. 7. The frontier molecular orbital in terms of HOMO and LUMO obtained at contour value of 0.02.

DNA [44,45]. Classically, it has been well accepted that hypochromism and bathochromism are the indications of non-covalent binding, however, hyperchromism is the indication of covalent binding [38,45]. As seen in Fig. 10(a & b), upon interaction of compound with Ct-DNA, the peaks in the range of 200–450 nm appeared, which underwent bathochromic shift with hypochromism, and this indicated the formation of compound-DNA adducts, mainly through non-covalent manner [43]. Present study showed the value of binding constant (K_b)1×10^5 l mol^{-1}. The lower value of K_b comparison to classical intercalators may be attributed to non-planarity in molecules [44] interestingly, same findings (grove binding) have been observed in the docking studies.

3.2. Cell cycle perturbation

3.2.1. Result & discussion

To assess the effect of compound **(3)** on cell cycle perturbation, the flow cytometry assay technique was performed against HepG2 and Siha cell lines. In present study, treated HepG2 cells at concentration ranges 10, 20 and 50 μM demonstrated the cell cycle phase distribution Fig. 11(a–d), 28%, 33% and 35% respectively arrest in G2/M as compared to untreated control (20.8%). However, treated Siha cells at concentrations 40 μM and 80 μM showed cell cycle distribution Fig. 11(e–g), 69%, 73.1% respectively arrest in G0/G1 as compared to untreated control (60%). Thus, these data suggested that compound **(3)** induces the cell cycle arrest G2/M phase and G0/G1 in HepG2 and Siha cells respectively.

3.3. Cytotoxicity studies

3.3.1. MTT assay

3-(4,5-dimethylthiazol-2-yl)-2,5-diphenyl tetrazolium bromide (MTT) is a vital dye reduced by the succinate dehydrogenase enzyme of mitochondrial living cells to produce water insoluble purple formazan crystals [46,47]. MTT assay has widely been used to demonstrate the cytotoxic effect of synthetic compounds/Natural compounds/Extract [48,49]. In the present study, MTT assay Fig. 12(a–e) revealed that compound **(3)** demonstrated cytotoxic effects against HepG2, Siha, Hela, MCF-7 and HEK-293 cells at different doses. The compound **(3)** displayed potent cytotoxic effect

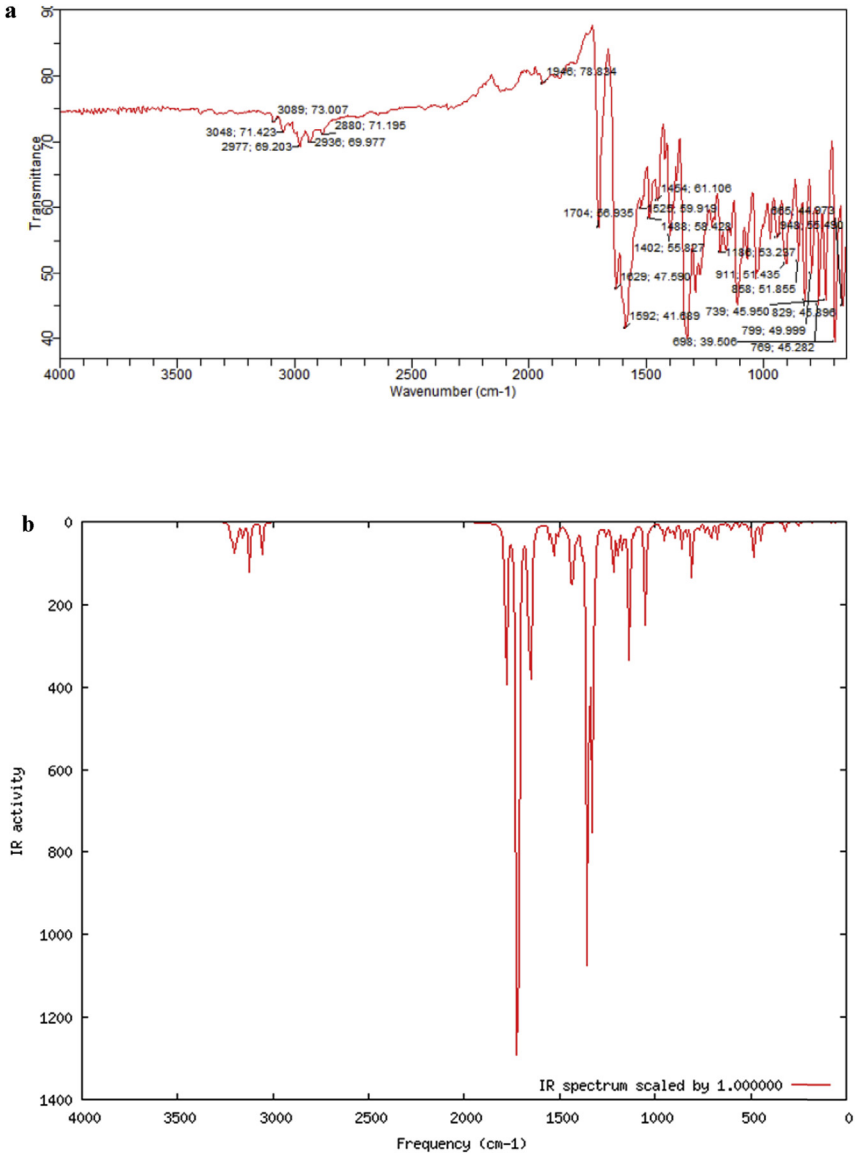

Fig. 8. Experimental and theoretical IR of compound**(3)**.

(**IC_{50} = 7.5 μM**) against HepG2 for 48 h treatment and, the IC_{50} against Hela, Siha and MCF-7 cells were found to be **74.83 μM, 66.98 μM** and **52.0 μM** Fig. 12(a–e). However, compound **(3)** showed lesser toxicity against HEK-293 (**287.89 μM**). The IC_{50} value of compound **(3)** against cancerous and non-cancerous cell also depicted in Table 5. Our results indicated that compound **(3)** was most active against HepG2 Cells followed by MCF-7, Siha and Hela, and lesser toxicity against HEK-293. So, compound **(3)** can be proven as better anticancer therapeutic agents.

3.4. Molecular simulation

3.4.1. DNA docking study

The computational studies have become a very prominent tool for drug discovery [50]. This is due to its low cost, rapid outcome, easy and free availability of many software's [51]. In order to verify our experimental results, DNA docking studies have been carried out using AutoDock tool [52,53]. The docking study of the compound was performed with DNA dodecamersd(CGCGAATTCGCG)2 (PDB ID:1BNA). The binding energy of the docked compound was observed as −7.18 kcal/mol. It was observed that the molecule preferred to interact with base pair of DNA and base of chain B and A as shown in Fig. 13(a). From the docking studies, it was also observed that molecule made a claw to inhibit the growth of DNA chain which might be better inhibitor as of cancer cells. Several polar and no-polar Fig. 13(b) interactions as given Table TS3. The oxygen atoms of thiazolidinone rings of compound **(3)** form four hydrogen bonds with moieties of chains A and B respectively. These typical docking observations were in good agreement with DNA binding experimental results. The phenomena can be explained by considering the non-covalent interactions such as hydrogen bonds, Van der Waal's forces, electrostatic and hydrophobic bonds. The docking energy (DGbinding) produced by AutoDock is sum of various factors as:

$$\Delta G_{binding} = \Delta G_{vdw} + \Delta G_{ele+} \Delta G_{h\ bond+} \Delta G_{desolv} + \Delta G_{tor}$$

Interestingly, it can be seen that, the sum of Vdw + Hb + dissolvation energy is quite high as **−9.40** kcal/mol. Electrostatic energy is **−0.16** kcal/mol. Torsional free energy is

Table 4
Comparison between experimental and theoretical (FT-IR) wave numbers (cm^{-1}) of compound**(3)** calculated by B3LYP level of theory.

Exp.wave no. in cm^{-1}	Calc.(Scaled) wave no. in cm^{-1}	Assignments
	558	τ(C34–C33–C35–C35–C36)20+τ(C39–C38–C41–C40)20+τ(C44–C43–C40–C41)20+Out(C41–C38–C45–C40)31
	533	δ(C48–C47–S5)22+σ(C24–C20–N7–C28)15+σ(C56–C52–N10–C50)15
	523	υ (S1–C32) 13+ υ (S5–C47)13+ δ (C48–C47–S5)13
	514	δ (C20–C28–N7) 17+ δ (C52–C50–N10)17
639	674	υ (S1–C32)28+ υ (S5–C47)28+ δ (C33–C32–S1)35
	648	δ(C48–N10–C49)11+δ(C36–C38–C40)11+δ(C40–C41–C43)11+ δ (C14–C16-c18)11
	644	δ(C4–C16–C18)21+(C14–C16–C18)21+δ(C61–C63–C65)21+ δ (C65–C67–C69)21
	624	δ(C4–C18–C16)44+(C11–C14–C16)25+δ(C4–C18–C16)19+ δ (C14–C16–C18)25
	604	τ (C30–N7–C31–C32) 10+ τ (C47–C48–N10–C49)12
665	709	τ (H15–C14–C16–C18)15+τ(H62–C61–C63–C65)15+τ (H64–C63–C65–C67)15+ τ (H68–C67–C69–C60)15
698		
739	742	υ (C32–C33)20+ υ (C33–C35)20+ υ (C35–C36)20+ υ (C40–C41)20+ υ (C40–C45)20
	735	σ (O2–C32–N7–C31)80
	725	σ (O2–C32–N7–C31)46+ σ (O6–C47–N10–C48)47
	770	τ (H9–C8–C11–C14)29+ τ (H12–C11–C14–C16)29+ τ (H15–C14–C16–C18)29
769	752	σ(O2–C32–N7–C31)35+ τ (C8–C11–C14–C16)+ τ (C32–C3–C34–C35)19+ τ (H36–C37–C38–C40)13
799	774	τ (H9–C8–C11–C14)26+ τ (H15–C14–C16–C18)53
	785	τ (H9–C8–C11–C14)20+ τ (H12–C11–C14–C16)20+ τ (H15–C14–C16–C18)20+τ(H17–C16–C18–C4) 20+τ(H62–C61–C63–C65)20
829	834	τ (H36–C37–C38–C40)70
	831	υ(C50–C52)24+υ(C33–C35)13+υ(C35–C36)13+ υ(C36–C38)13
	828	τ (H36–C37–C38–C40)86
	807	υ(C20–C28)19+υ(C24–C28)19+υ(C50–C52)19+υ(C50–C56)19
858	863	δ(C60–C61–C63)12+δ(C61–C63–C65)12+δ(C63–C65–C67)12+(δ C4–C18–C16)12+ δ (C11–C14–C16)12
	859	δ(C4–N3–C30)10+δ(C49–N13–C60)10+δ(N3–C30–N7)10+ δ (N10–C49–N13)10
	849	τ (H9–C8–C11–C14)82
904	918	τ (H9–C8–C11–C14)77
	905	δ (C4–N3–C30)13+ δ (C28–N7–C31)13+ δ (C4–N3–C30)13+ δ (N3–C30–N7)13+ δ (N10–C49–N13)13
	899	δ (C32–C31–O2)10+ (C47–C48–O6)10+ δ (N3–C30–N7)11
911	905	υ (C33–C35)22+ υ (C35–C36)22+ υ (C36–C38)22+ υ (C38–C40)22+ υ (C40–C41)22
	968	τ (H17–C16–C18–C4)56+ τ (H12–C11–C14–C16)14
	959	τ (H55–C52–C50–C56)29+ τ (H57–C56–C50– C52)29
	942	(H57–C56–C50–C52)11+τ(H56–C58–C50–C52)10
948	954	υ (C24–C28)43+ υ (N10–C50)26
950	947	τ (H51–C50–N10–C48)37+ τ (H53–C52–C50–C56)37
	940	τ (H34–C33–C35–C36)74
	936	υ (H34–C33–C35–C36)78
973	1054	δ (C11–C14)31+ δ (C14–C16)31+ τ (C16–C18)31
	1052	δ (H15–C16–C16)12+ υ (C14–C16)36
	1048	υ (C11–C14)12+ υ (C14–C16)12+ υ (C11–C14)12+ υ (C16–C18)12+ υ (C11–C14)12+ υ (C61–C63)12
	1029	δ (C36–C38–C40)74
	1170	δ (H39–C28–C40)40+ υ (H33–C37–C38)40
	1159	υ (C20–C28)49+ υ (C50–C52)49
	1136	υ(N3–C4)14+υ(N3–C30)14+υ(N7–C30)14+ υ (N7–C31)14
	1105	δ(H9–C8–C11)34+δ(H14–C15–C16)34+δ (H68–C67–C69)25
1186	1192	δ (H17–C16–C18)13+ δ (H62–C61–C63)22+ υ (H64–C63–C65)22+ υ (H66–C65–C67)22
	1185	δ (H9–C8–C11)71
	1266	υ (C32–C33)42+ υ (C33–C35)42+ δ (H36–C37–C38)19
	1255	δ (C33–C35–C36)14+ υ (C33–C35)25+ υ (C36–C38)25+ υ (C45–C47)25
	1222	δ(H42–C41–C43)22+δ(H34–C33–C35)22+υ(H37–C36–C38)22
	1219	υ(N3–C4)17+τ(H58–C56–C50–C52)13+δ(H20–C21–22)11+ δ (H22–C20–C23)11
	1217	δ(H44–C41–C43)25+δ(H34–C33–C35)13+δ(H39–C38–40)13
	1201	δ(H12–C11–C14)31+δ(H9–C8–C11)29+δ (H12–C11–C14)29
	1332	υ (C33–C35)32+ υ (C35–C36)32
	1327	υ (C61–C63)27+ υ (C63–C65)
	1326	υ (C60–C61)35+ υ (C4–C18)35
	1315	υ (N3–C4)51
	1385	υ (C32–C33)11+ υ (C33–C35)11+ υ (C40–C41)11+ υ (C45–C47)11+ υ (C41–C43)12
	1378	δ (H33–C34–C35)77
	1377	τ (H29–C28–N7–C30)36+ τ (H51–C50–N10–C48)11
	1377	τ(H26–C24–C28–C20)20+τ(H27–C24–C28–C20)+ τ(H29–C28–N7–C30)20
1402	1413	δ (H21–C20–H22)81
1454	1463	υ (C36–C38)44+ υ (C41–C43)44
1488	1490	δ(C12–C12–C14)11+δ(C11–C14–C16)+δ(C14–C16–C18)11+δ(C60–C61–C63)+δ(C61–C63–C65)11 δ (C63–C65–C67)11
1525	1532	δ (H9–C8–C11)46+ δ (H12–C11–C14)46
1592	1588	υ (C32–C33)65
1629	1630	υ (C4–C18)56

(*continued on next page*)

Table 4 (*continued*)

Exp.wave no. in cm^{-1}	Calc.(Scaled) wave no. in cm^{-1}	Assignments
1704	1783	υ (O2–C31)71
	1720	υ (N4–C4)74,
	1720	υ (N3–C4)73
2977, 2936	3055	υ (C20–H21)86
3054	3055	υ (C52–H53)83
3089	3059	υ (C20–H21)76

υ-stretching; δ-bending; τ-torsion, σ-out of plane.

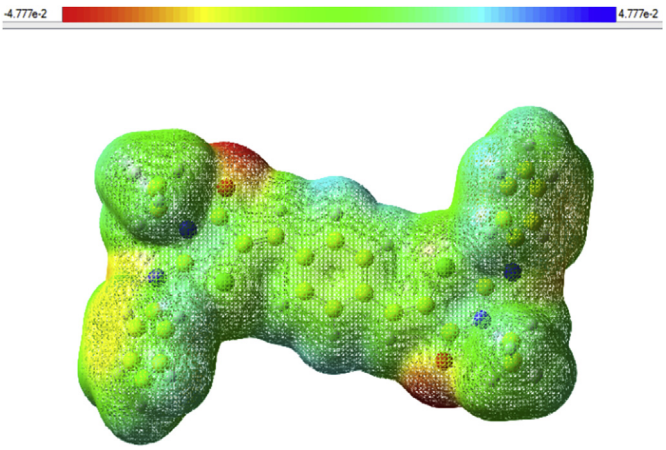

Fig. 9. Electron density mapped with electrostatic potential surface results to MEP.

2.39 kcal/mol. Finally docking energy is −**7.18** kcal/mol. It can be concluded that DNA binding is in good agreement with docking studies. The theoretical Free energy, Internal energy and Entropy was calculated to be −**1369.23** kcal/mol, −**5.0** kcal/mol and **4.58** kcal/mol/K at Temperature, T = 298.15 K.

3.4.2. Mechanism of action at supramolecular level

UV–Visible spectroscopic data exhibited that the compound **(3)** forms adducts with DNA due to covalent and non-covalent bindings. The docking studies also showed that the lead compound **(3)** interacted with the nucleic acid in the minor grooves of DNA. A deep imminent of interactions at supramolecular level was visualized and developed by docking studies. For this purposes 3-D docking models were developed for compound **(3)** and has been shown in Fig. 13(a). The keen evaluation and 3-D visualization of compound **(3)** model Fig. 13(a) showed that *N*-substituted phenyl ring, 4-thiazolidinone ring and 5-aryl groups are present in the minor grooves and the remaining parts are outside the grooves and binds with Chain B of DNA. The oxygen atom forms hydrogen bonds with **Guanine-cytosine and Adenine-thymine** base pairs Table TS3. So, it can be simply concluded that hydrogen bonding was the major force for the interactions of the compound **(3)** with DNA. The Vander Waal's force and steric effects also have a significant role in binding of ligand to the DNA. From the above results it could be concluded that the compound **(3)** has a greater affinity towards DNA, which is in accordance with the experimental UV–Visible spectroscopic data [56].

4. Conclusion

Compound **(3)** adopted (*Z, Z*)-configuration. The simulated DFT studies revealed that the experimental and theoretical investigations are in good agreement. The ionization energy of the compound **(3)**The binding energy of docked molecule with DNA (1BNA) was found to be −**7.18** kcal/mol. The DNA binding constant was found to be **1.0 x 10^5 Lmol^{-1}**. MTT assay reveals that compound **(3)** showed potential inhibitory activity against cancerous cells HepG2 pursued by MCF-7, Siha and Hela cells, and non-toxic effect against non-cancerous cells HEK-293. Cell cycle analysis (FACS) technique applied to HepG2 and Siha cells describe that G2/M cell cycle arrest was found in HepG2 cells, and G0/G1 cell arrest in Siha cells. Hence, it can be concluded that compound **(3)** possesses potent anti-cancer activity against HepG2 cell line.

5. Experimental protocol

All the required chemicals were purchased from Merck and Aldrich Chemical Company (USA). Precoated aluminium sheets

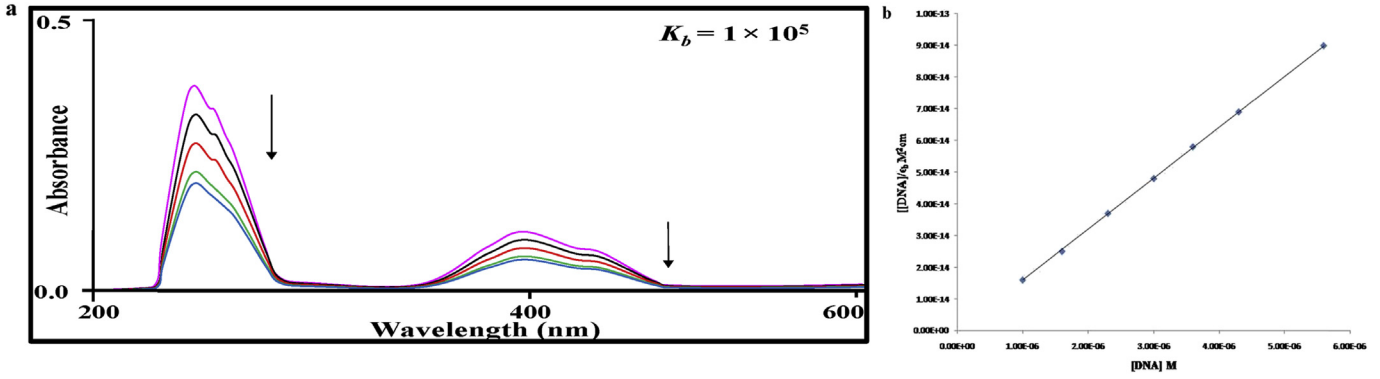

Fig. 10. (a–b): Absorption spectra of compound **(3)**; (a) DNA binding spectra of compound **(3)**, (b) DNA binding spectra of compound in the presence of increasing amount of Ct-DNA. Inset: plots of [DNA]/(ε_{a-} ε_f) (M^2 cm^{-1}) versus [DNA] for the titration of Ct-DNA with compounds. Experimental data points; full lines, linear fitting of the data. (Compound) 2.0 × 10^{-4} M, [DNA] 0.3–1.7 × 10^{-5} M.

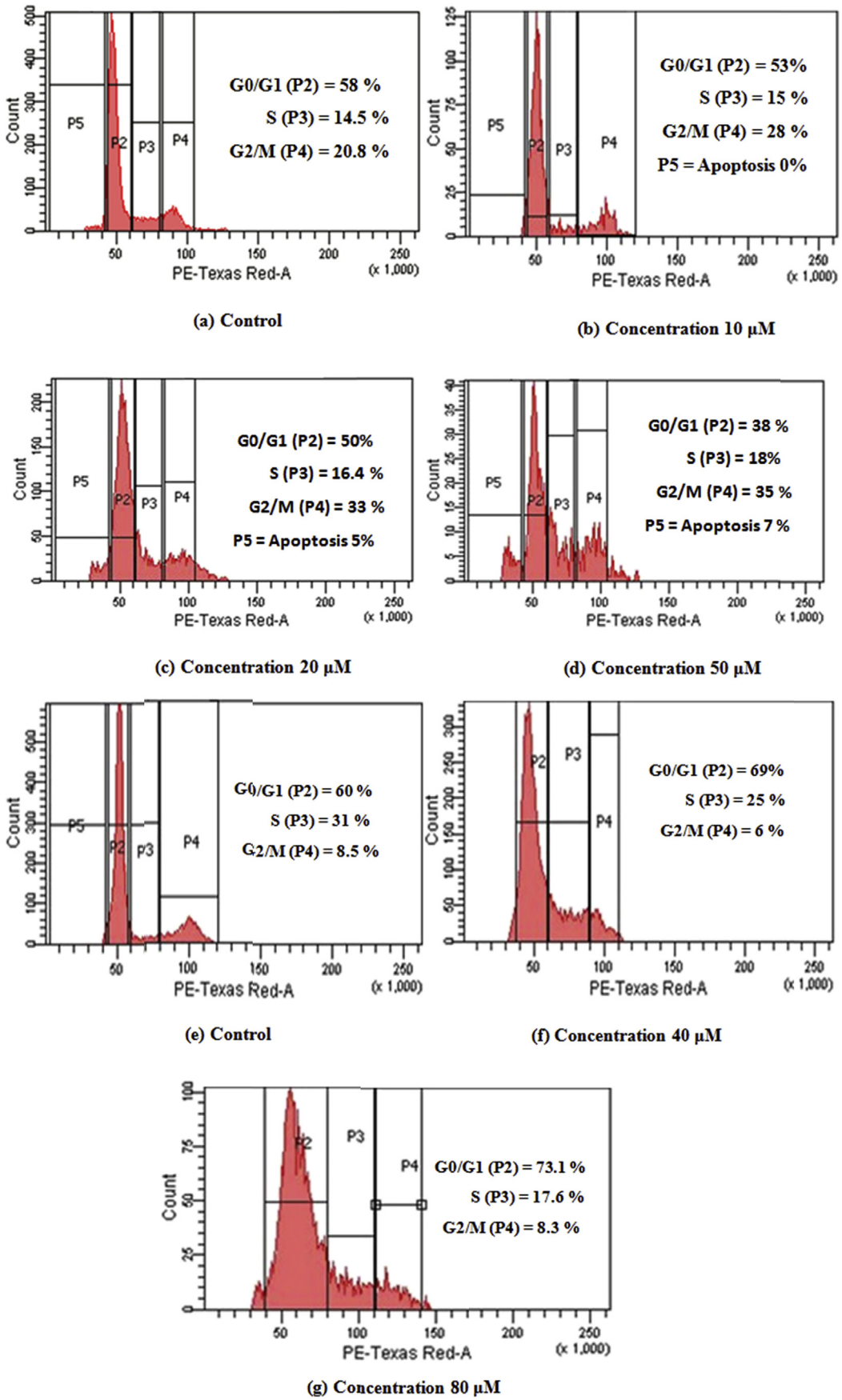

Fig. 11. (a–d): Cell cycle phase distribution against HepG2 cells with treatment of compound **(3)** having concentration 10 µM, 20 µM and 50 µM for 48 h (e–g): Cell cycle phase distribution against Siha cells at concentrations 40 µM & 80 µM for 48 h.

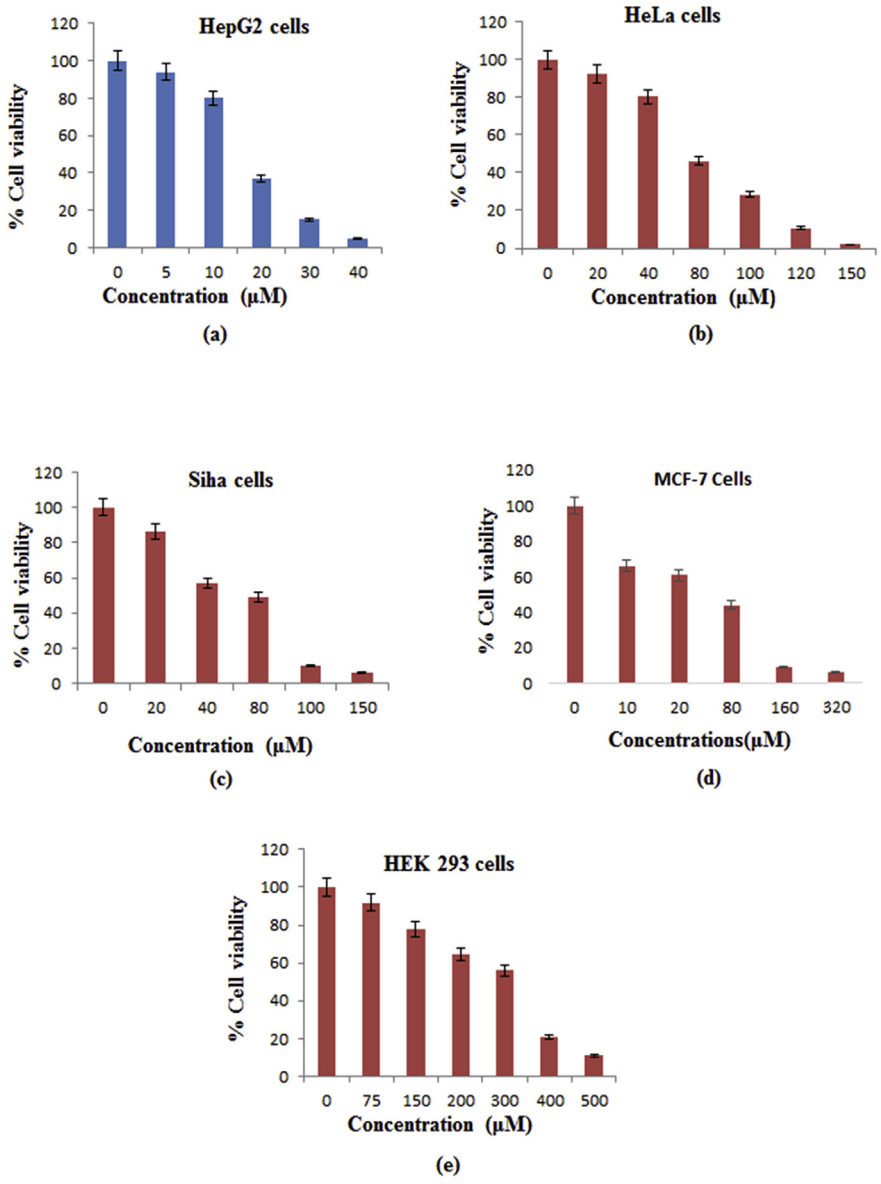

Fig. 12. (a–e): Percentage cells viability against (a) HepG2 (b) Hela (c) Siha (d) MCF-7 Cells (e) HEK-293.

Table 5
IC_{50} Values of the compounds **(3)** against HepG2, Siha, Hela, MCF-7 and HEK-293 normal human cells lines, and standard against HepG2 and MCF-7 cells.

S. No	Name of cell lines	Compound [3](IC_{50})	Doxorubicin (IC_{50})
1.	HepG2	7.5 (μM)	3.0(μM)
2.	MCF-7	52.0(μM)	8.1(μM)
3.	Hela	66.98(μM)	ND
4.	Siha	74.83 (μM)	ND
5.	HEK-293	287.89(μM)	ND

(Silica gel 60 F254, Merck Germany) were used for thin-layer chromatography (TLC) and spots were visualized under UV light. Ct-DNA (as sodium salt) was obtained from SRL Pvt. Ltd, Mumbai, India. The concentrations of DNA were determined spectrometrically with an extinction coefficient of 6600 M^{-1} cm^{-1} at 258 nm. Elemental analysis was carried out on CHNS Elementar analyzer (Vario EL-III) and the results were within ±0.3% of the theoretical values. FT-IR spectra were recorded on Perkin Elmer model 1600 FT-IR RX1 spectrophotometer as KBr discs. ^{1}H NMR and ^{13}C NMR spectra were recorded on Bruker Spectrospin DPX 300 MHz using $CDCl_3$ as a solvent and trimethylsilane (TMS) as an internal standard. Splitting patterns are designated as follows; s, singlet; d, doublet; m, multiplet. Chemical shift values are given in ppm. The ESI-MS was recorded on micrOTOF-Q II 10330 Electronspray ionization mass spectrometer (Bruker). X-ray data were collected on Bruker SMART Apex CCD diffractometer (SAI, Universidade da Coruña).

5.1. General procedure for the synthesis of 1-isopropyl phenylthiourea

Phenylisothiocyanate (1 mmol) was dissolved in toluene and then isopropyl amine (1 mmol) was added slowly at room temperature. After 5 min, the white precipitation appeared. Stirring was continued for 1 h. The precipitate was collected by filtration, washed with toluene, and dried to afford product (95.0%) as white powder.

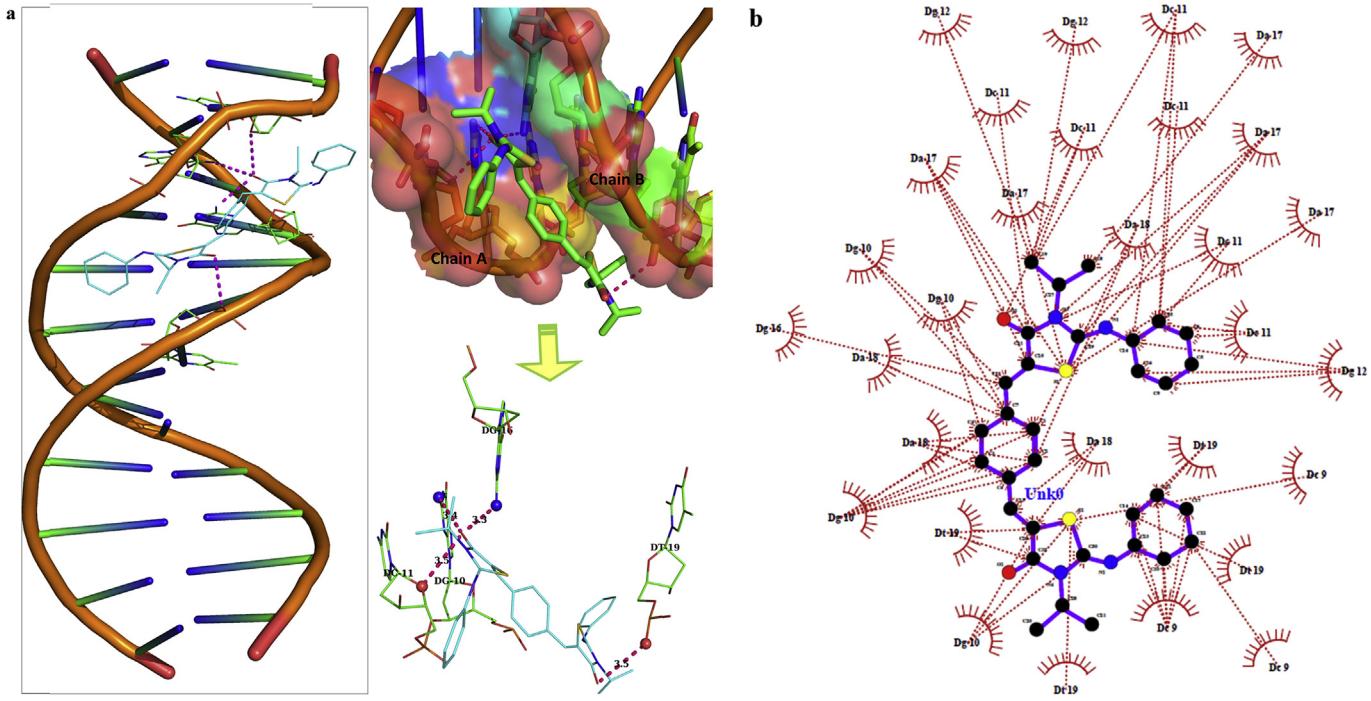

Fig. 13. (a & b): (a): 3-D representation of polar interactions of compound **(3)** with DNA(1BNA) (b) and hydrophobic interactions (i&ii) of DNA with compound **(3)**.

5.1.1. *1-Isoprppyl-3-phenylthiourea (1)*

Yield 95%. m.p: 125–128 °C; I.R λmax (cm^{-1}): 3265.14 (–NH), 3010.03 (C–H, Ar–H), 1240.83 (C=S); ^{1}HNMR ($CDCl_3$) δ (ppm): 7.461 (t, 2H, J = 7.5 Hz, Ar–H), 7.317 (t, 1H, J = 8.7 Hz, Ar–H), 7.220 (d, 2H, J = 7.8 Hz, Ar–H), 8.267 (s, 1H, NH), 5.873 (d, 1H, J = 6.0 Hz, NH), 4.62–4.55 (m, 1H, CH),1.218 (d, 6H, J = 6.3 Hz, $(CH_3)_2$); ^{13}C NMR ($CDCl_3$) δ (ppm): 178.94(C=S) (136.07, 130.12, 126.96, 124.88, Aromatic), 47.28 (CH), 22.27 ($(CH_3)_2$C).

5.2. General procedure for the synthesis of thiazolidinone

(2.120 g, 16.08 mmol) 1-isopropyl-3-phenylthiourea was dissolved in absolute ethanol. (1.643 g, 32.17 mmol) anhydrous sodium acetate and (1.190 g, 20.10 mmol) chloroacetic acid were added in a sequence. The suspension was refluxed for 12 h. The completion of the reaction was monitored by TLC plate. After the completion of the reaction, solvent was evaporated on rotator vacuum. In a reaction mixture, water was added and the aqueous layer was back-extracted with ethyl acetate. The organic layer was washed with saturated sodium bicarbonate and brine. The combined organic extracts were dried over Na_2SO_4, filtered through cotton, and concentrated in vacuum, after the concentration the mustard-oil like liquid product was obtained which on crystallization light brown solid was obtained in two weeks.

5.2.1. 3-Isopropyl-2-(phenylimino)thiazolidin-4-one(2)

Yield 78%; m.p. 128–130 °C; I.R λmax (cm^{-1}): 1715.24 (C=O), 1627.65 (C=N), 766.72 (C–S–C), 1370.65 (Ter. amine);^{1}HNMR ($CDCl_3$)δ (ppm); 7.36–7.29 (m, 2H, Ar–H), 7.15–7.08 (m, 1H, Ar–H), 6.952 (d, 2H, J = 7.8 Hz, Ar–H), 4.91–4.82 (m, 1H, CH), 3.701 (s, 2H, CH_2), 1.527 (d, 6H, J = 6.9 Hz, $(CH_3)_2$C); ^{13}C NMR ($CDCl_3$) δ (ppm): 171.84 (C=O) 154.08 (–C=N–), (148.92, 129.12, 124.35, 120.78, 119.73, Aromatic), 47.86 (CH), 24.38 ($(CH_3)_2$C).

5.3. General procedure of synthesis of bisthiazolidinone derivative

(2.0 mmol)-3-isopropyl-2-(phenylimino)thiazolidin-4-one, was dissolved in absolute ethanol in a round bottom flask. (1 mmol) terephthaladehyde was added followed by the addition of (2.30 mmol) hexahydropyridine to the reaction mixture. The reaction mixture was refluxed for 11–12 h. The reaction mixture was cooled to room temperature and the yellow precipitated solid was collected by filtration, washed with ethanol.The product was recrystallized in a chloroform and methanol at room temperature. The shining yellow crystal was obtained.

5.3.1. (2Z,2′Z,5Z,5′Z)-5,5′-(1,4-phenylenebis(methanylylidene)) bis(3-isopropyl-2-(phenylimino)thiazolidin-4-one) (3)

Yield: 85%; Anal. Calc: $C_{32}H_{30}N_4O_2S_2$; C 67.82, H 5.34, N 9.89, S 11.32%. found: 67.76, H 5.36, N 9.72, S 11.05%; IR λ_{max} (cm^{-1}): 3015.20 (Ar–H), 1692.25 (C=O), 1612.29 (C=N), 744.04 (C–S–C), 1330.95 (Ter. amine), 1525.70 (C=C); ^{1}HNMR ($CDCl_3$) δ (ppm); 7.631 (s, 2H, H–C=C-) 7.42–7.37 (m, 8H, Ar–H), 7.25–7.19 (m, 2H, Ar–H), 6.99 (d, 4H, J = 7.8 Hz, Ar–H), 5.07–4.97 (m, 2H, CH), 1.60 (d, 12H, J = 6.3 Hz (CH_3)C); ^{13}C NMR ($CDCl_3$) δ (ppm): 166.56 (C=O), 149.46 (C=N), 148.26 (C=C), 130.28 (C=C–S–), 134.69, 129.38, 128.70, 124.85, 123.28, 122.56 (aromatic), 48.19 (C–N), 18.97 (CH3); ESI: m/z: [M+H]+; 567.186; [M+2H]+: 568.1916, [M+3H]+: 569.1845.

6. X-ray crystal structure determination

Three-dimensional X-ray data were collected on a Bruker Kappa Apex CCD diffractometer at low temperature for **3** by the ϕ-ωscan method. Reflections were measured from a hemisphere of data collected from frames, each of them covering 0.3° in ω. 108647 reflections measured were corrected for Lorentz and polarization effects and for absorption by multi-scan methods based on symmetry-equivalent and repeated reflections. Of them, 5630 independent reflections exceeded the significance level ($|F|$/

$\sigma|F|) > 4.0$. After data collection, in each case a multi-scan absorption correction (SADABS) [57] was applied, and the structure was solved by direct methods and refined by full matrix least-squares on F^2 data using SHELX suite of programs [58] Hydrogen atoms were located in difference Fourier map and left to refine freely except for C(7), C(8), C(26) and C(27), which were included in calculation position and refined in the riding mode. Refinements were done with allowance for thermal anisotropy of all non-hydrogen atoms. A final difference Fourier map showed no residual density in the crystal: 0.319 and −0.195 e.Å^{-3}. A weighting scheme $w = 1/[\sigma^2(F_o^2) + (0.044700\ P)^2 + 1.021100\ P]$, was used in the latter stages of refinement. Further details of the crystal structure determination are given in Table 6. CCDC 1061909 contains the supplementary crystallographic data for the structure reported in this paper. These data can be obtained free of charge via http://www.ccdc.cam.ac.uk/conts/retrieving.html, or from the Cambridge Crystallographic Data Center, 12 Union Road, Cambridge CB2 1EZ, UK; fax: (+44) 1223 336 033; or e-mail: deposit@ccdc.cam.ac.uk. Supplementary data associated with this article can be found, in the online version, at http://dx.doi.org/10.1016/j.molstruc.2016.07.089.

Table 6
Crystal Data and Structure Refinement for compound **(3)**.

Compound code, Identification code	3
Formula	$C_{32}\ H_{30}\ N_4\ O_2\ S_2$
Formula weight	566.72
T, *K*	100
Wavelength, Å	0.71073
Crystal system	Monoclinic
Space group	$P2_1/c$
a/Å	10.9878(7)
b/Å	9.3077(6)
c/Å	28.3996(17)
β/°	93.170(3)
V/Å^3	2900.0(3)
Z	4
F_{000}	1192
D_{calc}/g cm^{-3}	1.298
μ/mm^{-1}	0.220
θ/(°)	1.44 to 26.49
R_{int}	0.0250
Crystal size/mm^3	0.44 × 0.32 x 0.23
Goodness-of-fit on F^2	1.055
$R_1[I > 2\sigma(I)]$[a]	0.0296
wR_2 (all data)[b]	0.0823
Largest differences peak and hole (eÅ^{-3})	0.319 and −0.195

[a] $R_1 = \sum||F_o| - |F_c||/\sum|F_o|$.
[b] $wR_2 = \{\sum[w(|F_o|^2 - |F_c|^2|)^2]|/\sum[w(F_o{}^2)^2]\}^{1/2}$.

6.1. Cytotoxicity studies (MTT assay)

6.1.1. Cell culture

Human hepatocellular carcinoma cell line (HepG2), Cervical cancer cell line (Siha, Hela), Breast cancer cell (MCF-7) and Human Embryonic Kidney cell line (HEK-293) were procured from National Curator of Cell Sciences (NCCS) Pune, India. Cells were cultured in Dulbecco's modified Eagle's medium (DMEM) with 10% fetal bovine serum with 100 units/mL penicillin, 100 μg/mL streptomycin, and 2.5 μg/mL amphotericin B, at 37 °C in a relative humidity 80%, 5% CO_2. [59].

6.1.2. MTT assay

Cytotoxicity of compound (3)/Doxorubicin was evaluated through MTT (3-(4,5-dimethylthiazole-2-yl)-2,5-diphenyl tetrazolium bromide, M2128 Sigma Aldrich) assay on HepG2, Siha, HeLa, MCF-7 and HEK-293 cells. MTT is a validated assay for the *in vitro* cytotoxicity of any natural, synthetic compounds and extracts [60,61]. The cell count 1.2 × 10^4 cells/well were seeded in 96 well plate (150 μL/well). After the overnight incubation, cells were treated with different concentration of compound **(3)**/Doxorubicin for 48 h. After the 48 h of treatment, the medium was remove and incubated with 20 μL of MTT solution (5 mg/mL in Phosphate saline buffer) for 4 h. The formazan crystals were formed by mitochondrial enzyme reduction, finally solubilized in DMSO (150 μL/well) and absorbance was recorded at 570 nm through the Microplate reader (iMark, BIORAD, S/N 10321). Percent viability was defined as the relative absorbance of treated versus untreated control cells.

6.2. DNA binding

The stock solution of disodium salt of Ct-DNA was prepared in tris-HCl buffer (pH 7.2–7.3) and stored at 4 °C temperature. Once prepared, the stock solution was used within 4 days. The concentration of the solution was determined spectrometrically. The ratio of absorbance at 260 and 280 (≥1.8) indicated that DNA was sufficiently free of protein. The concentration of DNA was measured using its extinction coefficient at 260 nm (6600 M^{-1} cm^{-1}) after dilutions. For the titration purpose, DNA stock solution was diluted using tris-HCl buffer. The compounds were dissolved in minimum amount of DMSO (2.0 × 10^{-4} M). UV-is absorption spectra were recorded after each addition of different concentrations of DNA. Absorption titration was conducted by adding varying concentrations (0.3–1.7 × 10^{-4} M) of DNA. The intrinsic binding constant (Kb) was determined by Eq. (2), which was originally known as Benessi–Hilderbrand equation and further modified by Wolfe et al. [62].

$$[DNA]/(\varepsilon_a - \varepsilon_f) = [DNA]/(\varepsilon_a - \varepsilon_f) + 1/K_b\ (\varepsilon_b - \varepsilon_f) \quad (2)$$

where the apparent absorption coefficients $\boldsymbol{\varepsilon_a}$, $\boldsymbol{\varepsilon_f}$ and $\boldsymbol{\varepsilon_a}$ correspond to A obs/[compounds], the extinction coefficient for the compounds, and the extinction coefficient for the compounds in the fully bound form. In plots of [DNA]/($\varepsilon_a - \varepsilon_f$) versus [DNA], K_b is given in the ratio of the slope to intercept.

6.3. DNA docking studies

Docking studies were performed at Intel(R) Core(TM) i3 CPU (2.3 GHz) with XP-based operating system (Windows 2007). 3D Structure of the lead compound **(3)** was drawn by Mercury software using CIF file of crystal structure and saved in pdb file format. The preparation of the compounds were done by assigning Gastegier charges, merging non-polar hydrogens, and saving it in PDBQT file format using AutoDock Tools (ADT)4.2 [54,55]. The X-ray crystal structure of DNA (PDB ID: 1BNA) was obtained from the Protein Data Bank [Protein Data Bank. Available online at: http://www.rcsb.org/pdb]. Using ADT 4.2, DNA was saved in PDB file format leaving heteroatoms (water). Gastegier charges were assigned to DNA and saved in PDBQT file format using ADT. Preparation of parameter files for grid and docking was done using ADT. Docking was performed with Auto-Dock4.2 (Scripps Research Institute, USA), considering all the rotatable bonds of ligand as rotatable and receptor as rigid [63] Grid box size of 47 × 65 × 63 Å with 1.0 Å spacing was used that included the whole DNA. In the present work we describe a plug in for PyMOL which allows carrying out molecular docking, virtual screening and binding site analysis with PyMOL. The plug in represents an interface between PyMOL and two popular docking programs, Autodock [52,53], Autodock Vina [64] and also the extensive use of a Python script collection (Autodock Tools) [63].

6.4. Methodology of cell cycle analysis

Flow cytometry was performed for the analysis of cell cycle arrest according to the standard method [65]. The effect of compound **(3)** on cell cycle on Siha and HepG2 cell lines were analyzed by the flow cytometry. After reaching the 70% confluency cells were serum starved overnight and treated with compound **(3)** for 48 h in complete medium. The cells were trypsinised, washed two times with chilled PBS and centrifuged at 1500 rpm for 5 min. Further, 1 ml chilled 70% ethanol was added to the cell pellet drop wise and vortexed gently. The cells were incubated for 1 h at 4 °C. The cells were centrifuged at 2000 rpm for 5 min, the pellet was washed twice with PBS. The cells were resuspended in 500 μL PBS, added 10 μl ribonuclease (100 μg/mL final concentration) and incubated for 30 min at 370C. Cells were stained with propidium iodide (50 μg/mL final concentrations) and incubated for 15 min. Flow cytometry analysis was performed with FACS (Becton Dickinson). A minimum of 10,000 cells were acquired. Further, histogram was analyzed by Flowjo software for cell cycle analysis.

Acknowledgment

One of the authors Md. Mushtaque is highly thankful for financial assistance from UGC (UGC-BSR fellowship) and Chancellor Al-Falah University. The Author is also thankful to Dr. Amir Azam, Deptt. of Chemistry, Jamia Millia Islamia, New Delhi, India for his help in the process of synthesis and the Head, Deptt. of Biosciences, JMI, for his permission to work at Genome Biology Lab.

Appendix A. Supplementary data

Supplementary data related to this article can be found at http://dx.doi.org/10.1016/j.molstruc.2016.07.089.

References

[1] World Health Statistics, World Health Organization, Geneva, 2012, 2012.
[2] H. Guoa, H. Wua, J. Yanga, Y. Xiaoa, H.J. Altenbachb, G. Qiua, H. Hua, Z. Wua, X. Hea, D. Zhoua, X. Hua, Steroids 76 (2011) 709–723.
[3] F. Bray, A. Jemal, N. Grey, J. Ferlay, D. Forman, Lancet Oncol. 13 (2012) 790–801.
[4] M.K. Mallath, D. G Taylor, R.A. Badwe, G.K. Rath, V. Shanta, C.S. Pramesh, R. Digumarti, P. Sebastian, B.B. Borthakur, A. Kalwar, S. Kapoor, S. Kumar, J.L. Gill, M.A. Kuriakose, H. Malhotra, S.C. Sharma, S. Shukla, L. Viswanath, R.T. Chacko, J.L. Pautu, K.S. Reddy, K.S. Sharma, A.D. Purushotham, R. Sullivan, Lancet Oncol. 15 (2014) e205–212.
[5] F. Bray, B. Moller, Nat. Rev. Cancer. 6 (2006) 63–74.
[6] L.A. Shervington, N. Smith, E. Norman, T. Ward, R. Phillips, A. Shervington, Eur. J. Med. Chem. 44 (2009) 2944–2951.
[7] K. Loven, L. Stein, K. Furst, S. Levy, Clin. Ther. 24 (2002) 990–1000.
[8] A. Skladanowski, J. Konopa, Biochem. Pharmacol. 46 (1993) 375–382.
[9] R. Lesyk, B. Zimenkovsky, Curr. Org. Chem. 8 (2004) 1547–1577.
[10] R. Lesyk, O. Vladzimirska, S. Holota, L. Zaprutko, A. Gzella, Eur. J. Med. Chem. 42 (2007) 641–648.
[11] D. Havrylyuk, B. Zimenkovsky, O. Vasylenko, L. Zaprutko, A. Gzella, R. Lesyk, Eur. J. Med. Chem. 44 (2009) 1396–1404.
[12] D. Kaminskyy, B. Zimenkovsky, R. Lesyk, Eur. J. Med. Chem. 44 (2009) 3627–3636.
[13] O. Ates, H. Altıntas, G. Otuk, Arzneim. Forsch, Drug Res. 50 (2000) 569–575.
[14] A. Kocabalkanl, O. Ates, G. Otuk, Arch. Pharm. Med. Chem. 334 (2001) 35–39.
[15] S.G. Kucukguzel, E.E. Oruc, S. Rollas, F. Sahin, A. Ozbek, Eur. J. Med. Chem. 3 (2002) 197–206.
[16] V.S. Palekar, A.J. Damle, S.R. Shukla, Eur. J. Med. Chem. 44 (2009) 5112–5116.
[17] N. Cesur, Z. Cesur, N. Ergenc, M. Uzun, M. Kiraz, O. Kasımoglu, D. Kaya, Arch. Pharm. Weinh. 327 (1994) 271–273.
[18] N. Karali, E. Ilhan, A. Gursoy, M. Kiraz, Farmaco 53 (1998) 346–349.
[19] H.T.Y. Fahmy, Boll. Chim. Farm. 140 (2001) 422–427.
[20] M.L. Barreca, A. Chimirri, L.D. Luca, A.M. Monforte, P. Monforte, A. Rao, M. Zappala, J. Balzarini, E. De Clercq, C. Pannecouque, M. Witvrouw, Bioorg. Med. Chem. Lett. 11 (2001) 1793–1796.
[21] A. Rao, A. Carbone, A. Chimirri, E.D. Clercq, A.M. Monforte, P. Monforte, C. Pannecouque, M. Zappala, Farmaco 57 (2002) 747–751.
[22] A. Rao, A. Carbone, A. Chimirri, E.D. Clercq, A.M. Monforte, P. Monforte, C. Pannecouque, M. Zappala, Farmaco 58 (2003) 15–120.
[23] M.L. Barreca, A. Chimirri, E.D. Clercq, L.D. Luca, A.M. Monforte, P. Monforte, A. Rao, M. Zappala, Farmaco 58 (2003) 259–263.
[24] A. Rao, J. Balzarini, A. Carbone, A. Chimirri, E.D. Clercq, A.M. Monforte, P. Monforte, C. Pannecouque, M. Zappala, Farmaco 5 (2004) 33–39.
[25] L. Bukowski, M. Janowiec, Z. Zwolska-Kwiek, Z. Andrezejczyk, Pharmazie 53 (1998) 371–376.
[26] M. Mushtaque, F. Avecilla, A. Azam, Eur. J. Med. Chem. 55 (2012) 439–448.
[27] L. He, L. Zhang, X. Liu, X. Li, M. Zheng, H. Li, K. Yu, K. Chen, X. Shen, H. Jiang, H. Liu, J. Med. Chem. 52 (2009) 2465–2481.
[28] R. Ottana, R. Maccari, M.L. Barreca, G. Bruno, A. Rotondo, A. Rossi, G. Chiricosta, R. Di Paola, S.L. Sautebin Cuzzocrea, M.G. Vigorita, Bioorg. Med. Chem. 13 (2005) 4243–4252.
[29] L.J.S. Knutsen, C.J. Hobbs, C.G. Earnshaw, A. Fiumana, J. Gilbert, S.L. Mellor, F. Radford, N.J. Smith, P.J. Birch, J.R. Burley, S.D.C. Ward, I.F. James, Bioorg. Med. Chem. Lett. 17 (2007) 662–667.
[30] R. Moreno-Funquen, J.C. Castillo, R. Abonia, J. Ellena, A. Carlos, De Simone, Acta Cryst. E. 70 (2014) 1235–1236.
[31] K.N. Houk, S. Menzer, S.P. Newton, F.M. Raymo, J.F. Stoddart, D.J. Williams, J. Am. Chem. Soc. 121 (1999) 1479–1487.
[32] J.J. Novoa, F. Mota, Chem. Phys. Lett. 318 (2000) 345–354.
[33] B.D. Becke, Phys. Rev. A 38 (1988) 3098–3100.
[34] C. Lee, W. Yang, R.G. Parr, Phys. Rev. B 37 (1988) 785–789.
[35] M.J. Frisch, G.W. Trucks, H.B. Schlegel, G.E. Scuseria, M.A. Robb, J.R. Cheeseman, J.A. Montgomery, T. Vreven, K.N. Kudin, J.C. Burant, J.M. Millam, S.S. Iyengar, J. Tomasi, V. Barone, B. Mennucci, M. Cossi, G. Scalmani, N. Rega, G.A. Petersson, H. Nakatsuji, M. Hada, M. Ehara, K. Toyota, R. Fukuda, J. Asegawa, M. Ishida, T. Nakajima, Y. Honda, O. Kitao, H. Nakai, M. Klene, X. Li, J.E. Knox, H.P. Hratchian, J.B. Cross, C. Adamo, J. Jaramillo, R. Gomperts, R.E. Stratmann, O. Yazyev, A.J. Austin, R. Cammi, C. Pomelli, J.W. Ochterski, P.Y. Ayala, K. Morokuma, G.A. Voth, P. Salvador, J.J. Dannenberg, V.G. Zakrzewski, S. Dapprich, A.D. Daniels, M.C. Strain, O. Farkas, D.K. Malick, A.D. Rabuck, K. Raghavachari, J.B. Foresman, J.V. Ortiz, Q. Cui, A.G. Baboul, S. Clifford, J. Cioslowski, B.B. Stefanov, G. Liu, A. Liashenko, P. Piskorz, I. Komaromi, R.L. Martin, D.J. Fox, T. Keith, M.A. Al-Laham, C.Y. Peng, A. Nanayakkara, M. Challacombe, P.M.W. Gill, B. Johnson, W. Chen, M.W. Wong, C. Gonzalez, J.A. Pople, Gaussian 03, Revision E.01, Gaussian Inc, Pittsburgh, PA, 2003.
[36] J.P. Foster, F. Weinhold, J. Am. Chem. Soc. 102 (1980) 7211–7218.
[37] N. Sinha, O. Prasad, V. Narayan, S.R. Shukla, J. Mol. Simul. 37 (2011) 153–163.
[38] F.V. Lewis, C. Loannides, D.V. Parke, Xenobiotica 24 (1994) 401–408.
[39] B. Kosar, C. Albayrak, Spectrochim. Acta. A. 78 (2011) 160–167.
[40] M.J. Alam, S. Ahmad, Spectrochim. Acta. A. 136 (2015) 961–978.
[41] T.A. Koopmans, Physica 1 (1934) 104–113.
[42] B. Kosar, C. Albayrak, Spectrochim. Acta A 78 (2011) 160–167.
[43] J. Wang, X.R. Yang, Spectrochim. Acta A 74 (2009) 421–426.
[44] G. Zhang, X. Hu, P. Fu, J. Photochem Photobiol. B 108 (2012) 53–61.
[45] Y. Xu, D.D. Wang, X.J. Sun, S.Y. Zeng, L.W. Li, D.Z. Sun, Thermochim. Acta 493 (2009) 30–36.
[46] M.N. Patel, P.A. Parmar, D.S. Gandhi, A.P. Patidar, Spectrochimica Acta Part A Mol. Biomol. Spectrosc. 97 (2012) 54–59.
[47] Eric Long, K. Jacqueline Barton, Acc. Chem. Res. 23 (1990) 271–273.
[48] S.M. Thom, R.W. Horobin, E. Seidler, M.R. Barer, Appl. Bacteriol. 74 (1993) 433–443.
[49] S.R. Kim, M.J. Park, M.K. Lee, S.H. Sung, E.J. Park, Free Radic. Biol. Med. 32 (2002) 596–604.
[50] S.H. Kim, J.H. Zo, M.A. Kim, K.K. Hwang, I.H. Chae, Nutr. Res. 23 (2003) 1671–1683.
[51] H.Y. Lina, S.H. Juan, S.C. Shen, F.L. Hsu, Y.C. Chen, Biochem. Pharmacol. 66 (2003) 1821–1832.
[52] B. Kitchen, H. Decornez, J.R. Furr Bajorath, J. Nat. Rev. Drug Discov. 3 (2004) 935–949.
[53] G.M. Morris, D.S. Goodsell, D.S. Halliday, R. Huey, W.E. Hart, R. Belew, A.J. Olson, J. Comp. Chem. 19 (1998) 1639–1662.
[54] R. Huey, G.M. Morris, A.J. Olson, D.S. Goodsell, J. Comp. Chem. 28 (2007) 1145–1152.
[55] O. Trott, A. Olson, J. Comp. Chem. 31 (2010) 455–461.
[56] I. Ali, A. Haque, K. Saleem, M.F. Hsieh, Bioorg. Med. Chem. 21 (2013), 3808–3020.
[57] SHELX, G.M. Sheldrick, Acta Crystallogr. Sect. A 64 (2008) 112–122.
[58] M. Sheldrick, *SADABS*, Version 2.10, University of Göttingen, Germany, 2004.
[59] M.K. Gupta, T.V. Neelakantan, M. Sanghamitra, R.K. Tyagi, A. Dinda, S. Mualik, C.K. Mukhopadhyay, S.K. Goswami, Antioxi. Redox Signal 8 (2006) 1081–1093.
[60] S.J. Mehdi, A. Ahmad, M. Irshad, Cytotoxic effect of carvacrol on human cervical cancer cells, Biol. Med. 3 (2011) 307–312.
[61] M. Irshad, S.J. Mehdi, A.A. Al-Fatlawi, Phytochemical composition of cassia fistula fruit extracts and its anticancer activity against human cancer cell lines, J. Biol. Act. Prod. Nat. 4 (2014) 158–170.
[62] A. Wolfe, G.H. Shimer Jr., T. Meehan, Biochemistry 26 (1987) 6392–6396.
[63] M.F. Sanner, J. Mol. Graph Model 17 (1999) 57–61.
[64] M. Morris, G.S. Goodsell, R.S. Halliday, R. Huey, W.E. Hart, R. Belew, A.J. Olson, J. Comput. Chem. 19 (1998) 1639–1662.
[65] W.W. Lai, J.S. Yang, K.C. Lai, C.L. Kuo, C.K. Hsu, C.K. Wang, Rhein induced apoptosis through the endoplasmic reticulum stress, caspase-and mitochondria-dependent pathways in SCC-4 human tongue squamous cancer cells, Vivo 23 (2009) 309–316.